mAbs 6:6, 1509–1517; November/December 2014; Published with license by Taylor & Francis Group, LLC

Raman spectroscopy characterization of antibody phases in serum

Audrey E Baker[1,*], Amber R Mantz[2], and Mark L Chiu[1]

[1]Janssen R&D; Biotech CoE; Spring House, PA USA; [2]Janssen Supply Chain; Process Science and Advanced Analytics; Spring House, PA USA

Keywords: monoclonal antibody, inhomogeneity, miniature, droplets, phase separation, Raman spectroscopy, serum, confocal microscopy, circular dichroism

Abbreviations: mAb, monoclonal antibody; PBS, phosphate-buffered saline; β-sheet, beta-sheet; α-helix, alpha helix; CD, circular dichroism; HC-CDR, heavy chain complementarity-determining region

When administered in serum, an efficacious therapeutic antibody should be homogeneous to minimize immune reactions or injection site irritation during administration. Monoclonal antibody (mAb) phase separation is one type of inhomogeneity observed in serum, and thus screening potential phase separation of mAbs in serum could guide lead optimization. However, serum contains numerous components, making it difficult to resolve mAb/serum mixtures at a scale amenable to analysis in a discovery setting. To address these challenges, a miniaturized assay was developed that combined confocal microscopy with Raman spectroscopy. The method was examined using CNTO607, a poorly-soluble anti-interleukin-13 human mAb, and CNTO3930, a soluble anti-respiratory syncytial virus humanized mAb. When CNTO607 was diluted into serum above 4.5 mg/mL, phase separation occurred, resulting in droplet formation. Raman spectra of droplet phases in mixtures included bands at 1240 and 1670 cm^{-1}, which are typical of mAb β-sheets, and lacked bands at 1270 and 1655 cm^{-1}, which are typical of α-helices. The continuous phases included bands at 1270 and 1655 cm^{-1} and lacked those at 1240 and 1670 cm^{-1}. Therefore, CNTO607 appeared to be sequestered within the droplets, while albumin and other α-helix-forming serum proteins remained within the continuous phases. In contrast, CNTO3930 formed only one phase, and its Raman spectra contained bands at 1240, 1670, 1270 and 1655 $cm,^{-1}$ demonstrating homogeneous distribution of components. Our results indicate that this plate-based method utilizing confocal Raman spectroscopy to probe liquid-liquid phases in mAb/serum mixtures can provide a screen for phase separation of mAb candidates in a discovery setting.

Introduction

Recombinant monoclonal antibodies (mAbs) engineered for specificity and potency have provided therapies for numerous debilitating conditions.[1-3] Since the first approval of a mAb, muromonab-CD3 (Orthoclone OKT3®),[4,5] regulatory requirements have demanded increasingly extensive evaluation for safety and acceptable pharmacokinetic properties.[5] Poor mAb profiles that cause adverse drug reactions can be linked to suboptimal biophysical properties such as aggregation and inhomogeneity in serum.[6-10] MAbs with poor solubility in phosphate-buffered saline (PBS) can have improved solubility in an optimal formulation buffer. However, the homogeneity of this formulated mAb when mixed with serum has to be confirmed. Inhomogeneity in serum associated with mAb phase separation (also known as liquid-liquid phase separation) could affect drug distribution and cause irritation at the injection site.[11] Inhomogeneity is more likely to occur during high concentration dosing that are typical for intravenous intraperitoneal and subcutaneous administration. Therapeutic mAbs are formulated at a range of concentrations, and many, such as golimumab (Simponi®) and ustekinumab (Stelara®), are formulated near 100 mg/mL.[12,13] mAb concentration near the injection sites could be as high as the formulation concentration, but, as the mAb circulates in the body and becomes diluted with body fluids or distributed to anatomical sites, its concentration in serum decreases. As has been illustrated with rituximab,[14] the distribution of a typical therapeutic mAb is influenced by several factors, including drug pharmacokinetic and pharmacodynamic properties.[15-19]

As this study illustrates, the risk of phase separation in serum is greater at higher mAb concentrations, which would be expected near the site of administration. This study utilized

*Correspondence to: Audrey E Baker; Email: abaker8@its.jnj.com

Submitted: 06/11/2014; Revised: 08/26/2014; Accepted: 09/15/2014

http://dx.doi.org/10.4161/19420862.2014.975100

mAbs at concentrations >40 mg/mL, where phase separation is more likely to be seen. Better understanding of phase components will be required to understand the nature of the phase separations. Phase characterization requires an assay that can probe within liquid-liquid phases in <4 μL of sample and analyze molecular components, including mAb and serum molecules. Because serum contains many proteins, lipids and salts, analyzing liquid-liquid phases in serum is very challenging. Standard protein detection methods such as absorption spectroscopy, size exclusion chromatography, analytical ultracentrifugation and light scattering cannot resolve the protein components of mAb-serum mixtures in volumes as low as the 4 μL that would be needed for a phase separation assay used in a discovery setting.

Confocal microcopy utilizes pinholes in the optical train to selectively image specific depths within a sample. Raman spectroscopy probes the vibrational transitions of molecules, and thus provides a chemical fingerprint. Raman spectroscopy also identifies secondary, tertiary and quaternary structures of proteins. Uses for Raman analysis include monitoring protein structural changes in different formulation buffers[20-22] and evaluating proteins during crystallization.[23,24] Combining Raman spectroscopy with confocal microscopy allows for nondestructive chemical identification at specific locations within sample wells, including within liquid-liquid phases. We therefore coupled confocal microscopy to Raman spectroscopy to probe samples of less than 4 microliters to investigate phases formed in mAb/serum or mAb/buffer solutions. The method was also adapted to a 96-well plate for increased throughput. To distinguish between IgG and serum, the method relied on the spectral differences between the β-sheet structures of IgG and the α-helices of albumin to track these molecules within the phases. Secondary structures observed from Raman analysis were validated by comparing these with structures observed from circular dichroism (CD), which is another solution method for determining protein structures.[25] Using this technique, we described the distribution of the proteins within the different phases.

To develop an assay for phase separation in serum, we investigated 2 mAbs, CNTO607 and CNTO3930, with different biophysical profiles. CNTO607 is a human mAb that targets and neutralizes interleukin (IL)-13, a T-helper cell cytokine involved in mediating allergic inflammation and disease.[26] However, CNTO607 displays poor solubility in PBS and interacts both with itself and with polyclonal IgG.[27-29] Although this mAb can be formulated in sodium acetate pH 5 to improve concentratability for high concentration administration, there was a risk that CNTO607 would not remain soluble when introduced into serum. In contrast, CNTO3930, a humanized anti-respiratory syncytial virus mAb, is soluble in both PBS and sodium acetate and does not form liquid-liquid phases in serum. MAb concentrations needed in this assay were ≥50 mg/mL, which represents typical mAb formulations used for intraperitoneal or subcutaneous administration.[12-14]

Results

To determine the mAb concentration range where liquid-liquid phase separation occurs, CNTO607 was titrated in human serum. Human serum contains numerous components, including proteins (albumin at 35–50 mg/mL and IgGs at ~11 mg/mL), glucose and salts.[30-32] CNTO607/serum mixtures were prepared in a 96-well plate equipped with 4 μL wells permitting several samples to be examined in one plate. Two μL of CNTO607 at 0.6 to 25 mg/mL were mixed with 2 μL of human serum and examined for solution clarity. This low-volume format enabled analysis in a discovery setting where protein amounts are often limited. Microscopic images of mAb/serum mixtures within each well are shown in **Figure 1**.

The images in **Figure 1** show liquid-liquid phase separations in the form of oil-like droplets in CNTO607/serum mixtures at final mAb concentrations of 4.5 to 25 mg/mL. Droplets were absent from mixtures containing CNTO607 at 3.0, 1.9 and 0.6 mg/mL, as well as from buffer or serum alone (images not shown). No precipitation was observed. At a final concentration of 25 mg/mL, CNTO607 also formed droplets in rat serum (data not shown). Therefore, phase separation was observed in human serum containing CNTO607 above 4.5 mg/mL.

Raman spectroscopy imaging

Raman spectroscopy coupled with confocal microscopy was used to probe the continuous and droplet phases that formed in mixtures of mAb with rat serum. This analysis was used to determine how the mAb distributed within these phases. The main protein components in human serum are albumin and IgG (35–50 mg/mL and ~11 mg/mL, respectively);[30-32] and rat serum contains albumin at ~16–30 mg/mL and IgG at 0.8–2.5 mg/mL.[33] Since we observed droplet formation in both these sera, which have similar compositions of major protein components, the Raman spectroscopy imaging was performed only with rat serum. In order to obtain Raman spectra of the IgG/serum or IgG/buffer samples, background Raman signals were needed for signal subtraction. Background signals collected on an empty Corning plate sealed with ClearSeal film were of low intensity compared with sample signals, and these signals were subtracted from each sample spectrum during data processing. Samples prepared for Raman imaging included each mAb at final concentrations of 25–35 mg/mL, as these conditions not only provided better signals but were also aligned with high drug concentrations that can be present for subcutaneous and intraperitoneal dosing.[12-14] Images and spectra of each mAb, as well as each buffer and rat serum control, were collected and used to resolve the spectra of sample mixtures. Images and spectra for CNTO607 in sodium acetate or CNTO3930 in PBS, along with their formulation buffer controls are shown in **Figure 2**.

The buffer controls, sodium acetate pH 5 and PBS, each yielded single continuous phases, and each buffer spectrum was distinct from the spectrum of either mAb. The Raman spectrum of sodium acetate shown in **Figure 2A**(i) included a major band at 1645 cm^{-1} that could be attributed to water,[34] along with bands at 929, 1347 and 1416 cm^{-1} that were consistent with sodium acetate.[35] The Raman spectrum of PBS shown in **Figure 2B**(i) included a band at 989 cm^{-1} consistent with phosphate in PBS, along with the major band at 1645 cm^{-1} attributed to water.[34,36] CNTO607 and CNTO3930 in their respective formulations each exhibited one

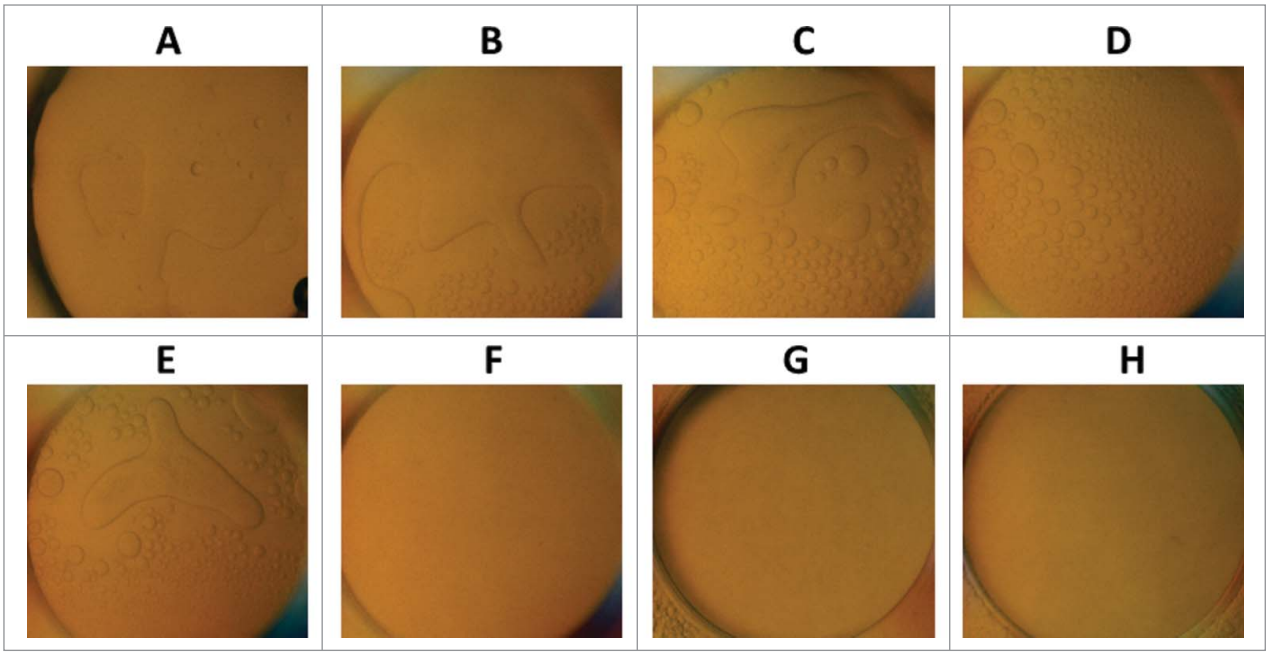

Figure 1. Micrograph images of CNTO607 in serum. CNTO607 titrations at total concentrations in serum at (**A**) 25 mg/mL, (**B**) 16.3 mg/mL, (**C**) 10.6 mg/mL, (**D**) 6.9 mg/mL, (**E**) 4.5 mg/mL, (**F**) 3.0 mg/mL, (**G**) 1.9 mg/mL, and (**H**) 0.6 mg/mL.

continuous phase (**Figure 2A**(iv,v) and **2B**(iv,v)), and spectra collected from the top and bottom of their respective wells were very similar. Spectra from both mAbs included bands at 1240 and 1670 cm^{-1} consistent with amide III and I bands, respectively, present in β-sheet or β-barrel structures, along with a band at 1004 cm^{-1} consistent with phenylalanine ring-breathing mode.[37,38] Additional bands at 1068 and 1138 cm^{-1} observed in the spectrum of CNTO607 could not be specifically assigned to known protein structures and were thought to be possibly spectral artifacts. Other bands present were not highlighted, but were generally consistent with those seen in protein spectra.[22-24] Based on the observed spectra, CNTO607 and CNTO3930 each formed a single phase in their respective formulation buffer and each contained β-sheet structures typical of IgG molecules.

CNTO607/PBS or CNTO607/serum mixtures produced droplet and continuous phases. To better differentiate these 2 phases, images and Raman spectra were collected. Images and spectra of CNTO607 mixtures are shown in **Figure 3A and 3B** respectively.

In order to assess each mAb, we prepared a sample set that included formulation buffer or diluent and serum controls, along with mixtures of the mAb with buffer or serum. The image of

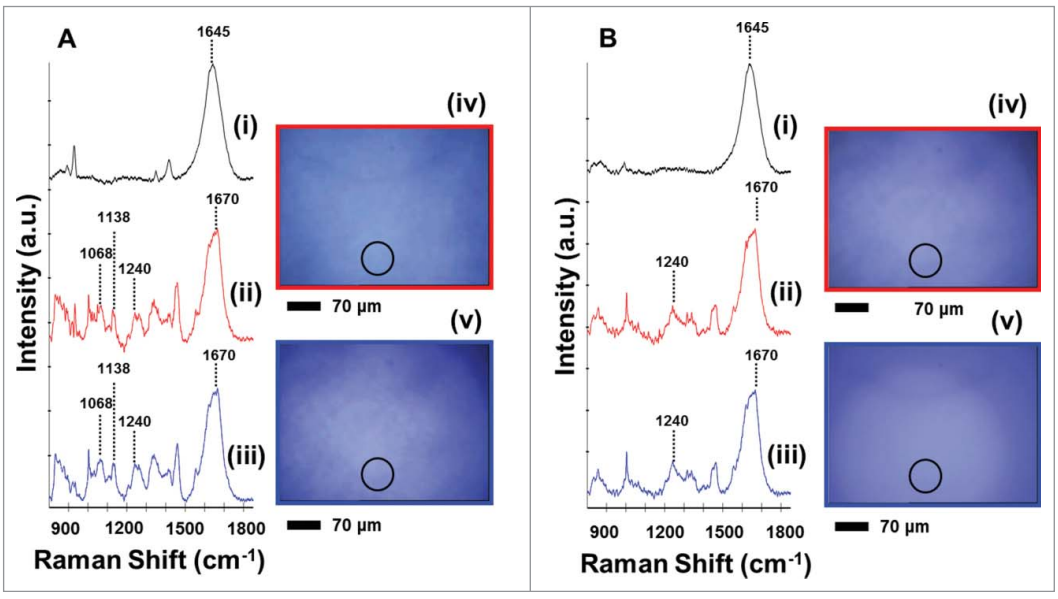

Figure 2. Raman spectroscopy images of **A**: CNTO607 in sodium acetate. **B**: CNTO3930 in PBS. (i) Spectrum of buffer controls: Sodium acetate (**A**) and PBS (**B**), (ii) spectra from the bottom of the wells, (iii) spectra from the top of the wells; (iv, v) corresponding representative images from the bottom and top of the wells. Black circles indicate positions where Raman spectra were collected.

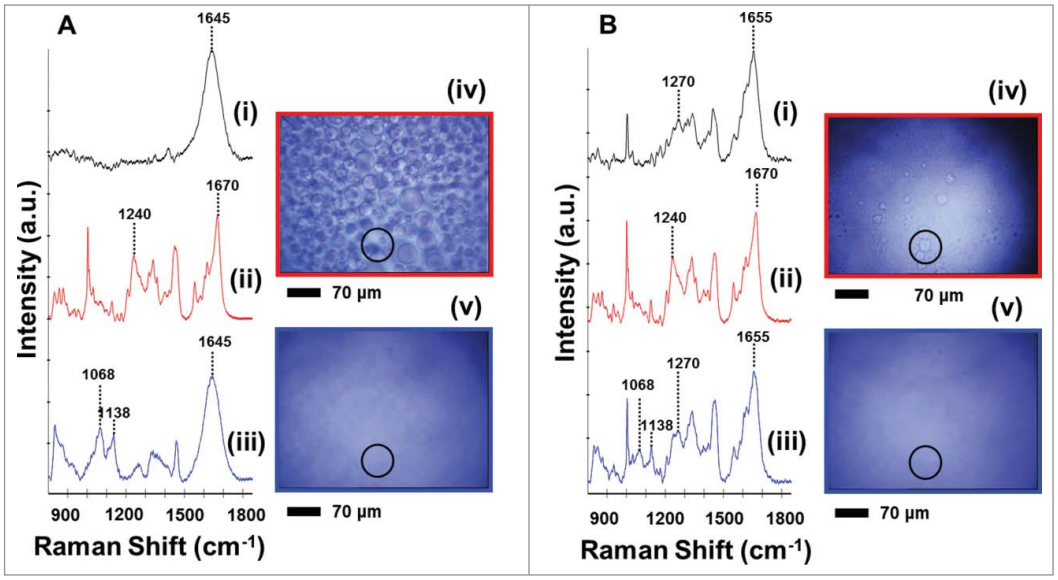

Figure 3. Raman spectroscopy images of **A**: CNTO607 in PBS. **B**: CNTO607 in serum. (i) Spectrum of diluent controls: NaAc/PBS (**A**) and NaAc/serum (**B**), (ii) spectra from within the droplet phases at the bottom of the wells, (iii) spectra from the continuous phase at the top of the wells, (iv) representative images from the bottom of the wells, and (v) representative images from the top of the wells. Black circles indicate positions where Raman spectra were collected.

the sodium acetate/PBS diluent control revealed a single continuous phase (not shown), and its corresponding spectrum is shown in **Figure 3A**(i). Sodium acetate/PBS spectrum included a band at 1645 cm^{-1} (water), and minor bands at 929, 1347 and 1416 cm^{-1} consistent with sodium acetate buffer. These intensities were comparatively lower than those previously shown (**Figure 2A**(i)) due to sample dilution. Images and spectra of CNTO607/PBS diluents are shown in **Figure 3A**(ii-v). Images revealed droplets near the bottom of the wells (**Figure 3A**(iv)) and clear continuous phases near the top of the wells (**Figure 3A** (v)). **Figure 3A**(ii) shows a representative spectrum from within the droplets. This spectrum included bands at 1004, 1240, and 1670 cm^{-1} consistent with β-sheet structures in IgG. The unassigned bands at 1068 and 1138 cm^{-1} previously seen in CNTO607 (**Figure 2A**(ii)-(iii)) were absent from the droplet spectrum. **Figure 3A**(iii) shows spectra from the corresponding continuous phase of the CNTO607/PBS diluent. This continuous phase exhibited a band at 1645 cm^{-1} (water), along with minor bands previously observed in the PBS control. In particular, this phase lacked bands at 1240 and 1670 cm^{-1} associated with IgG, but it included the unassigned 1068 and 1138 cm^{-1} bands that we considered to be an unknown artifact. Therefore, CNTO607 partitioned within droplets formed in the PBS diluent, while the continuous phase consisted mainly of buffer.

Images and spectra for CNTO607/serum diluents and the sodium acetate/serum control are shown in **Figure 3B**. The sodium acetate/serum control displayed only one phase (image not shown), and its spectrum included bands at 1655 and 1270 cm^{-1} indicative of an α-helical protein and consistent with serum albumin.[20-22] Images of CNTO607/serum diluents in **Figure 3B** (iv, v) revealed droplets near the bottom and a continuous phase near the top of the well. **Figure 3B** (ii) shows a representative spectrum from within the droplets. This spectrum included bands at 1004, 1240, and 1670 cm^{-1} consistent with β-sheet structures in IgG molecules. The 1068 and 1138 cm^{-1} bands previously seen in CNTO607 above were again absent from the droplet spectrum. **Figure 3B** (iii) shows the corresponding spectrum within the continuous phase of the CNTO607/serum diluent. This spectrum exhibited bands at 1270 and 1655 cm^{-1} observed previously in the serum control and was consistent with the amide III and I bands of an α-helical protein. The spectrum also included the band at 1004 cm^{-1} previously attributed to phenylalanine ring breathing,[20-22] and the 1068 and 1138 cm^{-1} artifact bands observed previously. As mentioned before, other bands present were not ascribed to particular structures. Based on the presence of the α-helix-associated amide I and III bands, the continuous phase was mainly serum albumin. Therefore, CNTO607/serum mixtures appeared to undergo phase separation to form droplets enriched with CNTO607 and a continuous phase enriched with albumin.

CNTO3930 is a mAb that displays solubility to at least 70 mg/mL in PBS. For analysis, it was diluted with sodium acetate to match the diluent composition of CNTO607. It was also diluted with serum to serve as a control mAb that does not form droplets in serum. Images and Raman spectra from CNTO3930 diluents with sodium acetate or serum are shown in **Figure 4A and 4B** respectively.

The sample set for CNTO3930 included PBS/sodium acetate buffer and serum controls, along with CNTO3930 in buffer or serum diluents. The sodium acetate spectrum is shown in **Figure 4A** (i), and it yields the expected bands similar to what was described previously. The images of the CNTO3930/sodium acetate sample showed clear continuous phases (**Figure 4A** (iv), (v)). Spectra from the top and bottom of the wells were similar and consistent with sample homogeneity. They included bands at 1240 and 1645 cm^{-1} and other unassigned protein bands consistent with IgG as described above (**Figure 4A** (ii, iii)). No phase separation or precipitation was observed with CNTO3930 in buffer. CNTO3930/serum images similarly revealed a single phase (**Figure 4B** (iv), (v)). Spectra from the top and bottom of the wells were similar and consistent with a single homogeneous phase (**Figure 4B** (ii), (iii)). Spectra included the characteristic

β-sheet bands at 1240 and 1670 cm^{-1}, although here the amide I band at 1670 cm^{-1} was present as a shoulder. The spectra also included bands at 1270 and 1655 cm^{-1} characteristic of α-helix amide III and I structures likely arising from albumin. Therefore, spectral results for mixtures of CNTO3930 and serum were consistent with evenly distributed IgG and albumin, characteristic of a homogeneous CNTO3930 mAb in serum.

The amide I and III Raman bands observed from the CNTO607 or CNTO3930 mixtures in buffer or serum are summarized in **Table 1**.

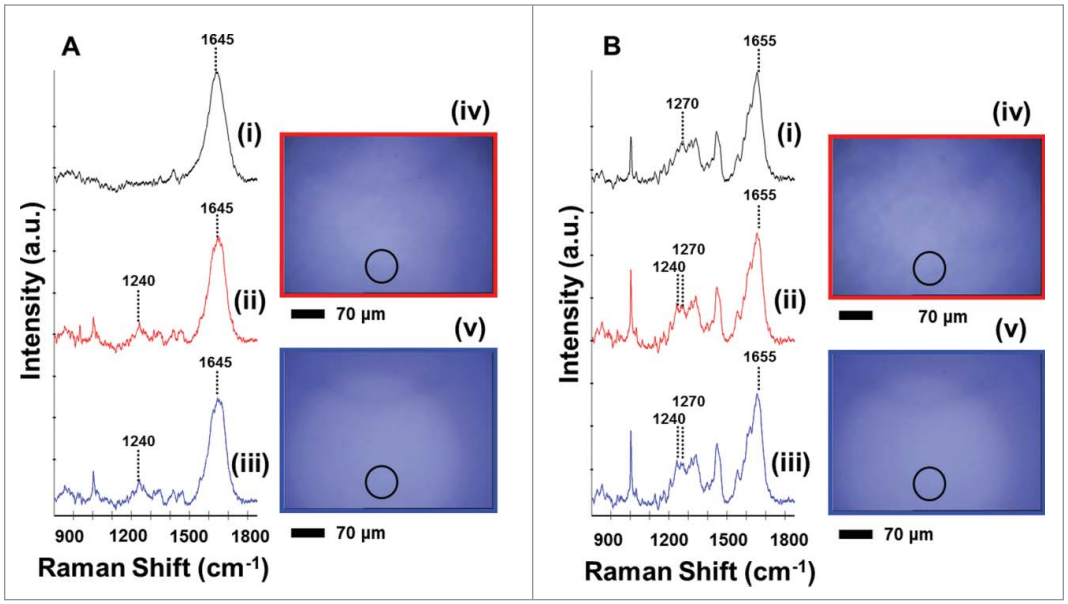

Figure 4. Raman spectroscopy images of **A**: CNTO3930 in sodium acetate. **B**: CNTO3930 in serum. (i) Spectrum of diluent controls: NaAc/PBS (**A**) and PBS/serum (**B**), (ii) spectra from the bottom of the wells, (iii) spectra from the top of the wells, (iv, v) representative images from the bottom and top of the corresponding well. Black circles indicate positions where Raman spectra were collected.

The CD spectra of each mAb, human serum albumin, and human serum were collected to determine their secondary structures and to help validate Raman secondary structure results. **Figure 5a** shows the CD spectra of CNTO607 and CNTO3930 evaluated in their respective formulation buffers.

While both PBS and sodium acetate buffers gave relatively flat spectra matching no distinctive secondary structures (not shown), the spectra of CNTO607 and CNTO3930 each showed a minimum near 217 nm and had similar peak magnitudes and shapes. Their spectra were characteristic of β-sheet secondary structures in proteins.[25] This observation was in agreement with deduced structures of the mAbs by Raman spectroscopy. **Figure 5b** shows the CD spectra of human serum albumin and human serum. These were obtained to help validate the observed secondary structures in serum from Raman spectroscopy. Since the major protein component of human serum was albumin, the spectrum of this protein was compared to the spectrum of serum. Based on an estimated serum protein concentration of ~50 mg/mL, serum was diluted 250 fold so it could be compared with human serum albumin. The spectrum of human serum albumin showed 2 minima at 208 and 222 nm typical of α-helical proteins including albumin.[25] The spectrum of human serum also showed minima at 208 and 222 nm, consistent with α-helical structures. The peak magnitudes differed because the serum protein concentration used was a calculated estimate. Human serum contains 35–50 mg/mL albumin and ~11 mg/mL IgG;[30-32] therefore, the similarity of its spectrum to that of albumin is consistent with its composition. These CD results were consistent with α-helical secondary structures in serum observed by Raman spectroscopy.

Discussion

The growing portfolio of therapeutic mAbs, as well as the growing sophistication and variety of antibody-derivatives being developed, demands improved technologies to demonstrate that

Table 1. Summary of Raman spectroscopy amide I and III bands observed in CNTO607 and CNTO3930 mixtures

			Secondary structure assignment for amide I		Secondary structure assignment for amide III	
mAb or reagent	**Diluent**	**Phase**	**Band Location (cm^{-1})**	**Structure**	**Band Location (cm^{-1})**	**Structure**
Serum	PBS	Continuous	1655	α-helix	1270	α-helix
CNTO607/ sodium acetate	PBS	Droplet	1670	β-sheet/barrel	1240	β-sheet/barrel
		Continuous	n/a		n/a	
	Serum	Droplet	1670	β-sheet/barrel	1240	β-sheet/barrel
		Continuous	1655	α-helix	1270	α-helix
CNTO3930/PBS	Sodium acetate	Continuous	1670	β-sheet/barrel	1240	β-sheet/barrel
	Serum	Continuous	1655, 1670	α-helix; β-sheet/barrel	1240, 1270	α-helix; β-sheet/barrel

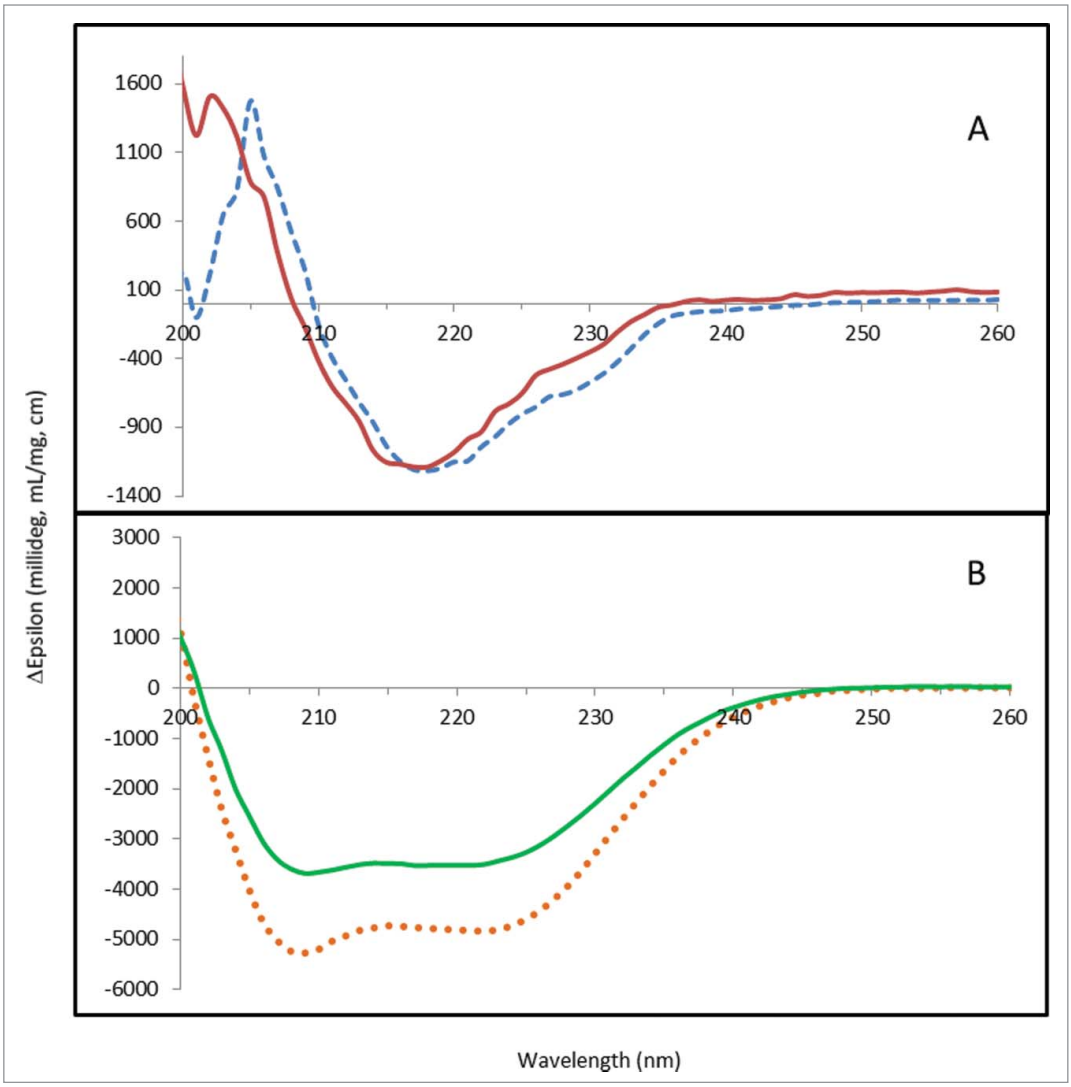

Figure 5. Circular dichroism spectra of **A**: CNTO607 (solid line) and CNTO3930 (dashed line) both at 0.2 mg/mL. **B**: Human serum albumin at 0.4 mg/mL (dotted line), and human serum diluted 250 fold in PBS (solid line).

these drugs possess desirable biophysical properties, including homogeneity or compatibility in serum. Such properties are desired to minimize potential risks associated with immunogenicity or inhomogeneity during drug administration.

Our results demonstrated that CNTO607 sequestered within droplets when diluted in PBS or in serum. The mechanism of droplet formation by CNTO607 was not fully understood; however, antibody liquid-liquid phase separation or gel formation has been observed during protein formulations and protein crystallization. In some studies, phase separation was correlated with decreased osmotic second virial coefficient (B_{22}) and increased protein-protein interactions.[39,40] Phase separation was also described as a form of reversible condensation arising from non-specific attractive interactions that are often superseded by aggregation, gelation or crystallization.[41] Wang et al. demonstrated that phase separation was induced by isothermal protein oligomerization.[42] He surmised that phase separation was related to excluded volume effects, influenced by the flexibility of the Fab arms of the antibody and possible effects of high concentrations on the shape. Phase separation observed from mAb-albumin mixtures used in their study were further associated with effective energies and the excluded volume entropies.[43] Phase separation is therefore associated with increased protein association, possible shape changes in concentrated solutions and solvent exclusion effects, although these will be highly dependent on the mAb structure and properties. CNTO607 had poor solubility in PBS, but could have higher solubility and show less protein-protein interactions when in sodium acetate buffer. However, use of alternate buffers did not resolve the phase changes that can occur when CNTO607 is mixed into serum.

Screening for mAb phase separation can also revealed how a droplet-forming mAb is distributed within the phases. This is valuable because protein clustering within droplets has been observed and associated with excluded volume effects and increased solution viscosity.[42,44] Therefore, providing a good description of phase separation can shed additional light into the biophysical behavior of the mAb.

A miniaturized Raman assay was developed to probe the composition of phases in mAb/serum or mAb/buffer mixtures. This plate-based method utilized <4 uL of sample for image and spectral analysis and a sealed 96-well plate where samples could be preserved and where multiple samples could be easily screened. Raman spectra were reproducible, well-resolved, and consistent with expected chemical composition or protein secondary structures, enabling differentiation between mAb, buffer, and serum components in mixtures. However, this method is not amenable to conditions where mAb concentrations are <10 mg/mL, as Raman signals are not sufficiently higher than buffer or serum IgG backgrounds. Data analysis was based on monitoring peaks associated with α-helices or β-sheets to distinguish between the mAb and albumin, the main serum component. The β-sheet

structures of CNTO607 and CNTO3930, and the α-helix structures of human serum albumin and human serum were corroborated using CD analysis.

A different approach would be needed to distinguish between proteins that possessed the same secondary structures. For instance, the spectra of CNTO607 and CNTO3930 both shared expected Raman β-sheet-amide bands, but they also showed spectral differences that likely reflected their unique amino acid compositions. These differences could be exploited to distinguish between similar types of molecules. While efforts could be made to identify other existing protein structures from the sample spectra, for the present application, focusing on protein bands specific to secondary structures and aligning sample data to those of the controls simplified the analysis and enabled us to distinguish between mAb and albumin in the phases.

Using this approach, the distribution of CNTO607 within phases was determined in sodium acetate, in PBS, and in serum through the β-sheet amide III and I bands at 1240 and 1670 cm^{-1}, respectively. These bands were observed within droplet phases and excluded from the continuous phases during phase separation. Within the continuous phases of CNTO607/serum samples, the 1270 and 1655 cm^{-1} bands associated with the α-helix amide III and I bands were attributed to serum albumin. Thus, at concentrations >4.5 mg/mL, CNTO607 sequesters within droplets, while albumin remains in the continuous phases.

We have shown that CNTO607 promotes phase separation in PBS and in serum and partitions within formed droplets. Previous studies on CNTO607 highlighted its poor solubility in PBS, and its tendency toward protein-protein interactions.[27] In addition, CNTO607 has an isoelectric point value of 7.4–7.5, which can contribute to its poor solubility in PBS and serum, as its net charge would be close to zero in these solutions.[29] CNTO607 also contains a hydrophobic region in its HC-CDR3. This hydrophobic region is associated with both binding to IL-13 and with non-specific cluster formation.[27,28] For mAbs that similarly display liquid-liquid phase separation and partition within droplets, we could reason that they may also display increased protein-protein interactions and other poor biophysical properties similar to those seen with CNTO607. CNTO3930 formed one phase in sodium acetate, PBS and serum and yielded spectra that represented the sum of all components in the mixture.

In conclusion, we developed a miniaturized plate-based assay that probes liquid-liquid phases in mAb solutions, generates spectral data for component identification, and provides a description of mAb distribution within the phases. Raman analysis provided the means to track the distribution of a mAb within liquid-liquid phases and relate the partitioning of the mAb to its biophysical properties. This assay could serve as a valuable screening tool for candidate serum incompatibility, and thus could be useful in the discovery of therapeutic mAbs.

Materials and Methods

CNTO607, which targets and neutralizes IL-13, is a human IgG1 mAb produced from an SP2/0 stable cell line by Centocor R&D. CNTO607 protein concentration was 50 mg/mL in sodium acetate pH 5. CNTO3930, which targets respiratory syncytial virus F, is a humanized IgG1 mAb produced by Sino Biological Inc. CNTO3930 protein concentration was 70 mg/mL in PBS.

Antibody phase-separation assessment

CNTO607 at 50.0 mg/mL in 50 mM sodium acetate, pH 5.0 was diluted serially with 50 mM sodium acetate, pH 5.0 to generate 8 mAb solutions from 50.0 to 1.2 mg/mL. Each sample was then further diluted 1:1 with human serum purchased from Bioreclamation (Hicksville, N.Y.), to yield final mAb concentrations of 25.0, 16.3, 10.6, 6.9, 4.5, 3.0, 1.9 and 0.6 mg/mL. 2 μL of each sample were pipetted into 4 μL wells of an HR8-142 96-Well Corning 3554 Crystal EX microplate (Hampton Research). Negative controls consisted of 2 μL of 50 mM sodium acetate pH 5.0 buffer or 2 μL of serum. To minimize sample evaporation, 50 μL of the 50 mM sodium acetate pH 5.0 buffer were added to the square center wells of the Corning plate, then the plate was sealed and incubated for 25 min at RT. Wells were imaged using a light microscope (Optical Apparatus Company) fitted with a Nikon SMZ 1000 lens at 10X magnification. Personal protective equipment were used during the handing of all serum samples.

Protein incubations and Raman imaging

Each mAb diluent was prepared in duplicate in a sample set that included pure diluent or pure serum. Sample sets included dilutions of CNTO607, (stock at 50 mg/mL in 50 mM sodium acetate pH 5.0), or CNTO3930 (stock at 70 mg/mL in PBS pH 7.4); PBS (Dulbecco's PBS: 2.7 mM KCl, 1.5 mM KH_2PO_4, 136.9 mM NaCl, 8.9 mM Na_2HPO_4-$7H_2O$) purchased from Invitrogen (Gibco, Grand Island, N.Y.); 50 mM sodium acetate, pH 5.0 or rat serum (Bioreclamation, Hicksville, N.Y.).

Each mAb and diluent was mixed at 1:1 (v/v) ratios in a final volume of 3 μL of solution. Samples were mixed in the 4 μL wells of a Corning Protein Crystallography plate (#3552, Corning Inc., Corning N.Y). Pure diluent (PBS, 50 mM sodium acetate, pH 5.0 or serum) were also added to plate wells. All samples were prepared in duplicate. The 96-well plate included reservoir wells that were filled with 50 μL of distilled water to minimize sample evaporation. After all reagents were added, the plate was sealed with ClearSeal film HR4-521 (Hampton Research) for Raman analysis. The plate was held at 4°C (for up to 2 d) prior to Raman imaging.

Confocal Raman Microscopy

A WITec Alpha 300 AR confocal Raman microscope equipped with a 532 nm excitation wavelength was used for all data collection. An excitation power of 31–32 mW was directed through a 20X/0.4 numerical aperture objective onto the samples. The Raman scattered light was collected by the same objective, then directed via a 50 μm optical fiber onto the charge-coupled device detector through a monochromator with an 1800 groove/mm rating. The number of spectral acquisitions ranged from 10–15, and data acquisition time was 30 s. Where only one continuous phase was present, micrograph images and spectra

were collected near the top and bottom of the solutions. Where multiple phases were present, micrograph images and spectra were collected from continuous, droplet or solid phases that may be present.

All data analyses were performed with WITec Project 2.08 software. Spectra were first treated by removing cosmic rays and subtracting background. Next, interference from the well plate or plate film collected on empty plate wells was subtracted from each sample spectrum. Spectral intensities were then normalized to the H_2O/amide I band maximum located between 1620 cm^{-1} and 1680 cm^{-1}.

Circular dichroism analysis

CNTO607 at 0.2 mg/mL in 50 mM sodium acetate pH 5.0 and CNTO3930 at 0.2 mg/mL in PBS were used for CD analysis. Three CD spectra were collected on each sample at 25°C in a 0.2 cm cell from 190 nm to 260 nm at 1 nm intervals with 1 sec signal averaging. Spectra of PBS and sodium acetate buffers were similarly collected. Human serum albumin that was free of globulin or fatty acid (Sigma-Aldrich) was diluted to 0.4 mg/mL in PBS, and 3 CD spectra were collected on each sample at 25°C in a 0.2 cm cell from 190 nm to 260 nm at 1 nm intervals with 1 sec signal averaging. Human serum (Bioreclamation) was diluted 1:250 in PBS for a final protein concentration of ~0.2 mg/mL, and CD spectra were collected using the conditions for human serum albumin and each mAb above. For data analysis, replicate CD spectra for each sample were averaged and converted to delta epsilon (millidegrees/(conc × path length × 32980) using the CDS software (Aviv Biomedical Inc.).

Disclosure of Potential Conflicts of Interest

No potential conflicts of interest were disclosed.

Acknowledgments

We acknowledge intellectual contributions and editorial comments from Yiqing Feng (Lilly Research Lab, Indianapolis, IN), Sarah Niesen (Janssen Supply Chain, Spring House, PA), and Mabel Cejas (J&J Consumer Products U.S., Fort Washington, PA).

References

1. Chames P, Van Regenmortel M, Weiss E, Baty D. Therapeutic antibodies: successes, limitations and hopes for the future. Br J Pharmacol 2009; 157 (2):220-33; PMID:19459844; http://dx.doi.org/10.1111/j.1476-5381.2009.00190.x
2. Nelson AL, Dhimolea E, Reichert JM. Development trends for human monoclonal antibody therapeutics. Nat Rev Drug Disc 2010; 9(10):767-74; PMID:20811384; http://dx.doi.org/10.1038/nrd3229
3. Lawrence S. Pipelines turn to biotech. Nat Biotechnol 2007; 25(12):1342; PMID:18066015; http://dx.doi.org/10.1038/nbt1207-1342
4. Smith SL. Ten years of Orthoclone OKT3 (muromonab-CD3): a review. J Transpl Coord 1996; 6(3):109-19; PMID:9188368
5. Van Wauwe JP, De Mey JR, Goossens JG. OKT3: a monoclonal anti-human T lymphocyte antibody with potent mitogenic properties. J Immunology 1980; 124 (6):2708-13
6. Daugherty AL, Mrsny RJ. Formulation and delivery issues for monoclonal antibody therapeutics. Adv Drug Deliv Rev 2006; 58(5-6):686-706; PMID:16839640; http://dx.doi.org/10.1016/j.addr.2006.03.011
7. Todd PA, Brogden RN. Muromonab CD3. A review of its pharmacology and therapeutic potential. Drugs 1989; 37(6):871-99; PMID:2503348; http://dx.doi.org/10.2165/00003495-198937060-00004
8. Moore WV, Leppert P. Role of aggregated human growth hormone (hGH) in development of antibodies to hGH. J Clin Endocrinol Metab 1980; 51(4):691-7; PMID:7419661; http://dx.doi.org/10.1210/jcem-51-4-691
9. Rosenberg AS. Effects of protein aggregates: an immunologic perspective. AAPS J 2006; 8(3):E501-7; PMID:17025268; http://dx.doi.org/10.1208/aapsj080359
10. Gamble CN. The role of soluble aggregates in the primary immune response of mice to human gamma globulin. Int Arch Allergy Appl Immunol 1996; 30(5):446-55; PMID:17728549; http://dx.doi.org/10.1159/000229829
11. Dimitrov DS. Therapeutic antibodies, vaccines and antibodyomer. mAbs 2010; 2(3):347-56; PMID:20400863; http://dx.doi.org/10.4161/mabs.2.3.11779
12. Janssen (2013, September 27). Stelara (ustekinumab) [Data sheet, CAS registry 815610-6-0]. Retrieved from "www.medsafe.govt.nzprofsDatasheetsstelarainj.pdf"
13. Janssen (2014, June 11). Simponi (Golimumab) [Data sheet, 140616 Simponi ads, CCDS 140407]. Retrieved from "www.medsafe.govt.nzprofsDatasheetssimponiinj.pdf"
14. Kagan L, Turner MR, Balu-lyer SV, Mager DE. Subcutaneous absorption of monoclonal antibodies: role of dose, site of injection, and injection volume on rituximab pharmacokinetics in rats. Pharm Res 2012; 29 (2):490-9; PMID:21887597; http://dx.doi.org/10.1007/s11095-011-0578-3
15. Schellkens H. Bioequivalence and the immunogenicity of biopharmaceuticals. Nature Rev Drug Disc 2002; 1 (6):457-62; PMID:12119747; http://dx.doi.org/10.1038/nrd818
16. Tabrizi M, Bornstein GG, Suria H. Biodistribution mechanisms of therapeutic monoclonal antibodies in health and disease. AAPS J 2010; 12(1):33-43; PMID:19924542; http://dx.doi.org/10.1208/s12248-009-9157-5
17. Johnson R, Wim J. Models for evaluation of relative immunogenic potential of protein particles in biopharmaceutical protein formulations. J Pharm Sci 2012; 101(10):3586-92; PMID:22736238; http://dx.doi.org/10.1002/jps.23248
18. Filipe V, Jiskoot W, Basmeleh AH, Halim A, Schellekens H, Brinks V. Immunogenicity of different stressed IgG monoclonal antibody formulations in immune tolerant transgenic mice. mAbs 2012; 4(6):740-52; PMID:22951518; http://dx.doi.org/10.4161/mabs.22066
19. Filipe V, Poole R, Oladunjoye O, Braeckmans K, Jiskoot W. Detection and characterization of subvisible aggregates of monoclonal IgG in serum. Pharm Res 2012; 29(8):2202-12; PMID:22467219; http://dx.doi.org/10.1007/s11095-012-0749-x
20. Lyng FM, Faolain EO, Conroy J, Meade AD, Knief P, Duffy B, Hunter MB, Byrne JM, Kelehan P, Byrne HJ. Vibrational spectroscopy for cervical cancer pathology from biochemical analysis to diagnostic tool. Exp and Mol Pathol 2007; 82(2):121-9; PMID:17320864; http://dx.doi.org/10.1016/j.yexmp.2007.01.001
21. Benevides JM, Overman SA, Thomas GJ Jr. Raman spectroscopy of proteins. Curr Protoc Protein Sci 2004; 33:17.8.1-17.8.35
22. Wen ZQ. Raman spectroscopy of protein pharmaceuticals. J Pharm Sci 2007; 96(11):2861-78; PMID:17847076; http://dx.doi.org/10.1002/jps.20895
23. Nitahara S, Maeki M, Yamaguchi H, Yamashita K, Miyazaki M, Maeda H. Three-dimensional Raman spectroscopic imaging of protein crystals deposited on a nanodroplet. Analyst 2012; 137:5730-5; PMID:23085689; http://dx.doi.org/10.1039/c2an35942a
24. Noda K, Sato H, Watanabe S, Yokoyama S, Tashiro H. Efficient characterization for protein crystals using confocal Raman spectroscopy. Appl Spectrosc 2007; 61 (1):11-8; PMID:17311710; http://dx.doi.org/10.1366/000370207779701514
25. Greenfield NJ. Using circular dichroism spectra to estimate protein secondary structure. Nat Protoc 2006; 1 (6):2876-90; PMID:17406547; http://dx.doi.org/10.1038/nprot.2006.202
26. Willis-Karp M, Chiaramonte M. Interleukin-13 in asthma. Curr Opin Pulmonary Med 2003; 9(1):21-7; PMID:12476080; http://dx.doi.org/10.1097/00063198-200301000-00004
27. Bethea D, Wu SJ, Luo J, Hyun L, Lacy ER, Teplyakov A, Jacobs SA, O'Neil KT, Gilliland GL, Feng Y. Mechanism of self-association of a human monoclonal antibody CNTO607. Protein Eng Des Sel 2012; 25:531-7; PMID:22915597; http://dx.doi.org/10.1093/protein/gzs047
28. Teplyakov A, Obmolova G, Wu SJ, Luo J, Kang J, O'Neil K, Gilliland GL. Epitope mapping of anti-interleukin-13 neutralizing antibody CNTO607. J Mol Biol 2009; 389(1):115-23; PMID:19361524; http://dx.doi.org/10.1016/j.jmb.2009.03.076
29. Wu SJ, Luo J, O'Neil KT, Kang J, Lacy ER, Canziani G, Baker A, Huang M, Tang QM, Raju TS, et al. Structure-based engineering of a monoclonal antibody for improved solubility. Protein Eng Des Sel 2010; 23 (8):643-51; PMID:20543007; http://dx.doi.org/10.1093/protein/gzq037
30. O'Connell TX, Horita TJ, Kasravi B. Understanding and interpreting serum protein electrophoresis. Am Fam Physician 2005; 71(1):105-12; PMID:15663032
31. Bossuyt X, Schiettekatte G, Bogaerts A, Blanckaert N. Serum protein electrophoresis by CZE 2000 clinical capillary electrophoresis system. Clin Chem 1998; 44 (4):749-59; PMID:9554485
32. Gonzalez-Quintela A, Alende R, Gude F, Campos J, Rey J, Meijide LM, Fernandez-Merino C, Vidal C. Serum levels of immunoglobulins (IgG, IgA, IgM) in a general adult population and their relationship with

alcohol consumption, smoking and common metabolic abnormalities. Clin Exp Immunol 2008; 151(1):42-50; PMID:18005364; http://dx.doi.org/10.1111/j.1365-2249.2007.03545.x
33. Zaias J, Mineau M, Cray C, Yoon D, Altman NH. Reference values for serum proteins of common laboratory rodent strains. J Am Assoc Lab Anim Sci 2009; 48 (4):387-90; PMID:19653947
34. Asher SA, Murtaugh JL; UV Raman excitation profiles of imidazole, imidazolium, and water. Appl Spectrosc 1988; 42(1):83-90; http://dx.doi.org/10.1366/0003702884428653
35. Ito K, Bernstein HJ. The vibrational spectra of the formate, acetate, and oxalate ions. Can J Chem 1956; 34 (2):170-8; http://dx.doi.org/10.1139/v56-021
36. Pye CC, Rudolph WW. An ab initio, infrared, and Raman investigation of phosphate ion hydration. J Phys Chem 2003; 107:8746-55; http://dx.doi.org/10.1021/jp035594h
37. Lu X, Liu Q, Benavides-Montano JA, Nicola AV, Aston DE, Rasco BA, Aguilar HC. Detection of receptor-induced glycoprotein conformational changes on enveloped virions by using confocal micro-Raman spectroscopy. J Virol 2013; 87(6):3130-42; PMID:23283947; http://dx.doi.org/10.1128/JVI.03220-12
38. Carter DC, Ho JX. Structure of serum albumin. Adv Protein Chem 1994; 45:153-203; PMID:8154369; http://dx.doi.org/10.1016/S0065-3233(08)60640-3
39. Dumetz AC, Chockla AM, Kaler EW, Lenhoff AM. Protein phase behavior in aqueous solutions: crystallization, liquid-liquid phase separation, gels, and aggregates. Biophysics J 2008; 94(2):570-83; PMID:18160663; http://dx.doi.org/10.1529/biophysj.107.116152
40. Le Brun V, Friess W, Schulz-Fademrecht T, Muehlau S, Garidel P. Lysozyme-lysozyme self-interactions as assessed by the osmotic second virial coefficient: Impact for physical protein stabilization. Biotechnology 2009; 4(9):1305-19; PMID:19579219; http://dx.doi.org/10.1002/biot.200800274
41. Wang Y, Aleksey Lomakin A, Hideshima T, Laubach JP, Ogun O, Richardson PG, Munshi NC, Anderson KC, Benedek GB. Pathological crystallization of human immunoglobulins. PNAS 2012; 109 (33):13359-61; PMID:22847421; http://dx.doi.org/10.1073/pnas.1211723109
42. Wang Y, Annunziata O. Liquid-liquid phase transition of protein aqueous solutions isothermally induced by protein cross-linking. Langmuir 2008; 24(6):2799-807; PMID:18229962; http://dx.doi.org/10.1021/la703223f
43. Wang Y, Lomakin A, Latypov RF, Benedek GB. Phase separation in solutions of monoclonal antibodies and the effect of human serum albumin. PNAS 2011; 108 (40):16606-11; PMID:21921237; http://dx.doi.org/10.1073/pnas.1112241108
44. Yearley EJ, Godfrin PD, Perevozchikova T, Zhang H, Falus P, Porcar L, Nagao M, Curtis JE, Gawande P, Taing R, Zarraga IE, Wagner NJ, Liu Y. Observation of small cluster formation in concentrated monoclonal antibody solutions and its implications to solution viscosity. Biophys J 2014; 106(8):1763-70; PMID:24739175; http://dx.doi.org/10.1016/j.bpj.2014.02.036